Materials Chemistry and Physics 314 (2024) 128853

Contents lists available at ScienceDirect

Materials Chemistry and Physics

journal homepage: www.elsevier.com/locate/matchemphys

Helichrysum arenarium-mediated facile green synthesis, antibacterial, catalytic activity and hydrogen evolution of metallic (Ag, Cu) and bimetallic (Ag/Cu) nanoparticles

Muradiye Şahin [a,b], Yasin Arslan [b,*], Ali Soyuçok [c]

[a] Institute of Science Kırşehir Ahi Evran University, 40100, Kırşehir, Turkey
[b] Department of Nanoscience and Nanotechnology, Burdur Mehmet Akif Ersoy University, Faculty of Arts and Science, 15030, Burdur, Turkey
[c] Agriculture, Livestock and Food Research and Application Center, Burdur Mehmet Akif Ersoy University, 15030, Burdur, Turkey

HIGHLIGHTS

- AgNPs, Ag/CuNPs and CuNPs were used for adsorption of CR and tested against the pathogenic microorganisms.
- Catalytic and sonocatalytic activities of nanoparticles for hydrogen evolution were investigated.
- Reusability and hot filtration tests were performed.

GRAPHICAL ABSTRACT

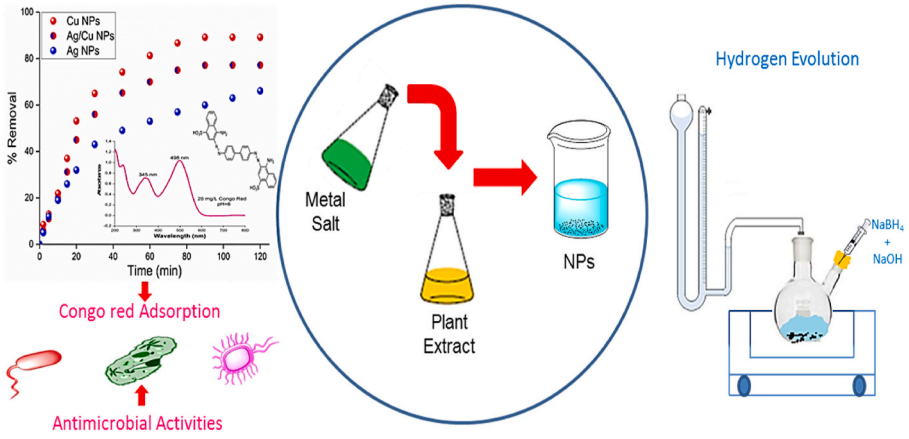

ARTICLE INFO

Keywords:
Adsorption
Green synthesis
Congo red
Hydrogen evolution
Antibacterial activity

ABSTRACT

Metallic Ag, Cu and bimetallic Ag/Cu nanoparticles (NPs) easily and economically synthesized by green synthesis method using *Helichrysum arenarium* plant extracts used as reducing agent were characterized with analysis of SEM (Scanning electron microscopy), TEM (Transmission electron microscopy) and BET (Brunauer-Emmett-Teller). The adsorption study of the synthesized nanoparticles for Congo Red (CR) azo dyestuff was carried out and dyestuff removal properties were investigated in detail. At 100 min, the CR removal percentages were found to be 90.2 %, 77.8 % and 66.1 % by Cu NPs, Ag/Cu NPs and Ag NPs, respectively and the adsorption was found to be in accordance with the second order kinetic model and Langmuir isotherm model. In reusability studies of Cu NPs adsorbent, CR removal was found to be 90.2 %, 88.9 % and 83.4 % in three experimental cycles, respectively. For antimicrobial activity of *Helichrysum arenarium* extract, Cu NPs, Ag/Cu NPs and Ag NPs were used to against 6 pathogenic microorganisms via disc diffusion assay. As a result of the antimicrobial assay, while *Helichrysum arenarium* extract did not show any effect against the tested pathogenic microorganisms, both Ag NPs

* Corresponding author.
E-mail address: yasinarslan@mehmetakif.edu.tr (Y. Arslan).

https://doi.org/10.1016/j.matchemphys.2023.128853
Received 8 October 2023; Received in revised form 14 December 2023; Accepted 22 December 2023
Available online 23 December 2023

and Ag/Cu NPs showed an inhibition zone diameter against the tested pathogenic microorganisms ($p < 0.05$). It is conceivable that it would be effective in controlling the growth of resistant microorganisms in aqueous media since it produces a similar level of inhibition in methicillin-resistant and non-resistant *S. aureus*. Finally, the catalytic activity of the synthesized nanoparticles was evaluated in hydrogen (H_2) production by hydrolysis of $NaBH_4$. Based on experimental results, the efficiency of hydrogen production was determined as Cu NPs > Ag/Cu NPs > Ag NPs. The optimum conditions for the highest yield of H_2 were investigated and the catalysis results were compared with sonocatalysis. This research shows that NPs can be synthesized in a simple, economical and environmentally friendly way and has a wide range of uses.

1. Introduction

Nanoparticles can find a place in many application areas owing to their unique properties, such as larger surface areas, larger surface charges, smaller sizes, higher reactivity, excellent morphological properties, amorphous and crystalline structures [1–4]. Metallic nanoparticles are widely used in catalyst synthesis, biosensor production studies, imaging and drug delivery systems, both medical and environmental applications, and electrical-electronic device component preparation [5–9]. The "Green Synthesis" method, in which various plant (leaf, fruit, bark, seed, etc.) extracts are used, has attracted as considerable attention in recent years due to the fact that compounds, such as polyphenols, polysaccharides, phenols, carboxylic acids, flavonoids, etc. act as reducing, capping and stabilizing agents in the synthesis of metal nanoparticles [10–13]. The green synthesis of metallic nanoparticles using plant extracts represents an advance over both chemical and physical synthesis methods because it is easy, simple, cost-effective and it is possible for large-scale nanoparticle synthesis. Furthermore, it not only eliminates the need for high energy, temperature and pressure but also eliminates the expensive, toxic and hazardous chemical reducing agents and toxic solvents. In principle, in the bioreduction mediated by a plant extract, the aqueous extract is mixed with an aqueous solution of the metal salt of interest. Metallic nanoparticles synthesized with plant extracts can be useful and effective in many applications, such as biosensor, biomedical, catalysis, adsorption, agriculture and antimicrobial [14–18]. In this research, both metallic and bimetallic nanoparticle synthesis using *Helichrysum arenarium* extract were carried out by using economical and environmentally friendly green method. Among metallic nanoparticles, while silver nanoparticles (Ag NPs) have a very high antibacterial effect [19,20], copper nanoparticles (Cu NPs) have antimicrobial, antifungal and antiviral properties [21,22].

As a result of the intensive development of the pharmaceutical, agricultural, textile and chemical industries, many chemical compounds reaching the aquatic environment, such as pesticides, steroid hormones, antibiotics or dyestuffs, cause severe pollution to water bodies in the worldwide and pose a serious health risk factor [23–26]. Synthetic dyes are among the most widely discharged pollutants due to their large-scale production and use in many industries, such as food, textiles, paper, leather, cosmetics, pharmaceuticals and plastics [23,24,27]. Due to their carcinogenic, teratogenic, mutagenic, toxic and allergic effects, dyestuff pollution in water can be dangerous for aquatic organisms [24,27–29] and can also damage the kidney, lung, liver, brain, reproductive and central nervous system through the food chain [27,30,31]. Therefore, it has become a necessity for the environment and public health to treat wastewater containing dyes before it is released into the environment [31–33]. Researchers are working on the effective removal of pollutants using one method or a combination of different methods. Versatile techniques including physical, chemical and biological methods are being investigated as efficient and economical alternatives [34]. In the removal of dyestuffs from wastewater, some physical, chemical and biological treatment methods, such as electrochemical process [35], coagulation-flocculation [36], photocatalysis [37], membrane separation [38], adsorption [39], ion exchange, oxidation, advanced oxidation processes, biodegradation [26,40,41] are applied. Among these methods, adsorption method stands out with its some advantages, such as being economical, easy applicability, high efficiency, ease of regeneration and no pre-treatment [42]. Among all types of dyes, azo dyes, which are the most widely produced and used, are highly resistant to heat, light and oxidizing agents. Azo dyes can be degraded into toxic amino acids by human intestinal flora and into carcinogenic amines by bacteria in human skin [43]. In this study, it was aimed to remove Congo red (CR), an azo dye, from aqueous media by adsorption using metallic and/or bimetallic nanoadsorbents. In addition, the antibacterial activity of all synthesized nanoparticles against to 6 pathogens was investigated in order to obtain healthier and better quality water.

Renewable energy sources, such as hydrogen, wind, geothermal, tidal, hydroelectric and solar energy should be used to save the world from increasing global warming to find a permanent solution to increasing energy demand and to limit the use of fossil fuels [44,45]. Hydrogen has the potential to be the energy source of the future compared to other energy sources [46]. Hydrogen production by hydrolysis of sodium boron hydride is both environmentally friendly and stable. Cu NPs, Ag NPs and Ag/Cu NPs will be used as nanocatalysts to increase the efficiency in the hydrogen production. In heterogeneous catalyst, the interaction takes place on the surface. Therefore, the performance of the heterogeneous catalyst depends on the activity of the surface area to which the substrate is exposed [47,48]. The exposed surface area increases as the active particle size decreases; however, very small particles have a high tendency to agglomerate. This is one of the most important problems that reduce the effectiveness of the heterogeneous catalyst. Most of the new technologies developed in the catalytic process are based on increasing the effective surface area as well as preventing agglomeration [49,50]. For this purpose, nanocatalysts synthesized to increase the catalytic effect were subjected to ultrasonication and hydrogen production rates were compared.

This research presents the effect of both metallic and bimetallic nanoparticles synthesized from plant extract against pathogenic microorganisms, comprehensive adsorption kinetics and equilibrium modeling of CR, and comparison of both catalytic and sonocatalytic activity in hydrogen production by $NaBH_4$ hydrolysis. Moreover, this study elucidates the reusability of Cu NPs as both catalyst and adsorbent.

2. Materials and methods

2.1. Synthesis and characterization of AgNPs, CuNPs and Ag/CuNPs

All nanoparticles were synthesized under the same optimum conditions (298 K, 5–10 mL extract, 0.1 M of 50 mL metal salt, 30 min and 500 rpm) as described in our study on drug removal from *Helichrysum arenarium* plant extract [51]. Silver nitrate ($AgNO_3$) was obtained from Fluka and Copper (II) sulfate pentahydrate ($CuSO_4 .5H_2O$) was obtained from Indosaw. TEM (Jeol JEM-1400 Plus), SEM-EDX (Carl Zeiss EVO-LS 10) and BET (Quantachrome Quadrasorb SI Brunauer-Emmett-Teller) analysis of the synthesized nanoparticles were performed. Ultrapure water (18MΩ·cm, PURIS Purification System) was used at every stage of the all experimental studies.

2.2. Adsorption experiments

Congo red ($C_{32}H_{22}N_6Na_2O_6S_2$) was obtained from Merck. Optimum

Table 1
Tested pathogen microorganisms.

Tested pathogen microorganisms
Salmonella Typhimurium ATCC 14028
Staphylococcus aureus ATCC 43300 [Methicillin-resistant *Staphylococcus aureus* (MRSA)]
Escherichia coli ATCC 25922
Listeria monocytogenes ATCC 19115
Staphylococcus aureus ATCC 25923
Staphylococcus epidermidis ATCC 12228

pH (2−10), initial dye concentration (10–50 mg/L) and adsorbent amount (10–50 mg) were determined using batch adsorption method. Adsorption isotherm and kinetic studies were carried out at three different temperatures, such as 298 K, 313 K and 328 K, at initial concentrations of 2–250 mg/L CR and for 150 min. The amount of CR remaining in aqueous solution was calculated from the calibration graph by taking measurements at 498 nm with UV–Vis spectrophotometer (Shimadzu UV-1800).

2.3. Antimicrobial activity studies

2.3.1. Disc diffusion method

The antimicrobial activities of *Helichrysum arenarium* extract and synthesized nanoparticles were tested against to six pathogenic microorganisms given in Table 1. These pathogenic microorganisms were grown as 18 h at 37 °C on Tryptic Soy Agar (Merck, Germany). Turbidity of microorganisms was adjusted to 0.5 McFarland via a densitometer (Biosan, Latvia) in 0.9 % of NaCl (Merck, Germany). 100 μL of 18 h fresh cultures adjusted to 0.5 McFarland were inoculated onto Mueller Hinton II Agar, Cation-Adjusted (Merck, Germany). After adding 30 μL of *Helichrysum arenarium* extract, Cu NPs, Ag/Cu NPs and Ag NPs into 6 mm empty sterile discs (Whatman™ 2017-006), the discs were placed in Petri dishes and the pathogenic microorganisms were incubated at 37 °C for 24 h. The diameters of the inhibition zones were measured with a millimeter ruler (CLSI, 2021).

2.3.2. Statistical analysis

The significant differences among results were determined using the IBM ® SPSS ® Statistics (IBM, U.S.A) package program version 25. By applying the analysis of variance (One-way ANOVA) to antimicrobial activity assay, the differences among the treatment groups were determined by Duncan multiple comparison test. In addition, the Pearson Correlation Test was used to determine both the relationships of treatment groups and pathogen microorganisms with each other. The antimicrobial study was performed in triplicate replications and the results were given as mean ± standard deviation.

2.4. Hydrogen production experiments

Sodium borohydride ($NaBH_4$) was obtained from Fluka and NaOH (sodium hydroxide) from Sigma-Aldrich. The system used for hydrogen production by hydrolysis of $NaBH_4$ consists of a two-neck flask, a gas burette and a shaking water bath. In the hydrolysis reaction, NaOH must be added to the medium to prevent the spontaneous degradation of $NaBH_4$ molecules in the solution and to ensure stability. The synthesized nanocatalysts were subjected to ultrasonication and their catalytic and sonocatalytic activities were compared under optimum conditions. Volume/time graphs were created by following the repulsion of water in the burette by the gas released as a result of the catalytic reaction. Optimum conditions were determined by optimization studies with the nanocatalyst that gave the best results in terms of NaOH amount (30–50 mg), nanocatalyst amount (25–100 mg), temperature (30–60 °C) and $NaBH_4$ amount (50 mM–100 mM).

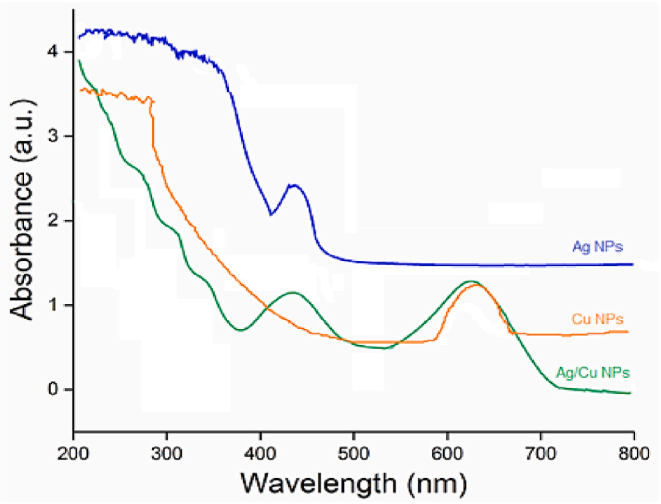

Fig. 1. UV–Vis spectra of all nanoparticles synthesized from *Helichrysum arenarium* plant extract.

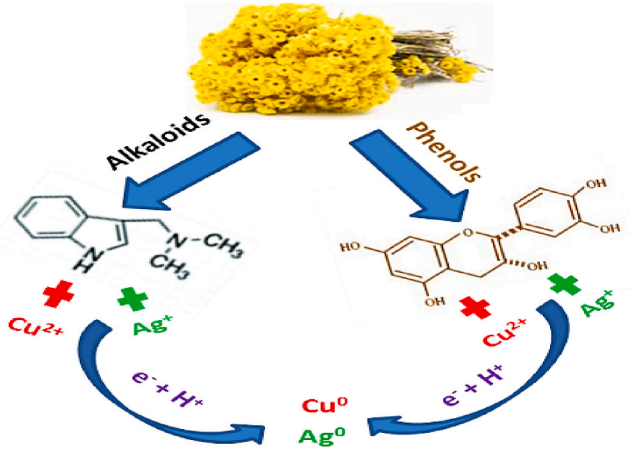

Fig. 2. A possible mechanism for green synthesis of Cu NPs and Ag NPs from *Helichrysum arenarium* plant extract. (For interpretation of the references to colour in this figure legend, the reader is referred to the Web version of this article.)

3. Results and discussion

3.1. Characterization of metallic and bimetallic nanoparticles

The characteristic peaks of both Ag and Cu NPs in the UV–Vis shown in Fig. 1 indicate that the nanoparticles were successfully synthesized [51,52]. From the FTIR spectra given in our previous study [51], it was understood that *Helichrysum arenarium* plant extract is an effective reducing and capping agent with amine and phenol groups in nanoparticle formation. According to both this result and the literature studies [17,53,54], the possible mechanism of nanoparticle synthesis with green method is given in Fig. 2.

The results of SEM-EDX and TEM analysis to elucidate the morphological properties, elemental composition and size of the synthesized Cu NPs, Ag/Cu NPs and Ag NPs are given in Fig. 3. SEM images confirmed the presence of rough and hollow surfaces with clustering and EDX images confirmed the presence of high elemental silver and copper peaks. Rectangular different patterns appear due to the clustering of nanoparticles on top of each other and the presence of extract on the particle surface [55]. In the EDX analysis of Ag/Cu and Cu NPs (Fig. 3b and c), S element is observed, which is thought to be due to the metal

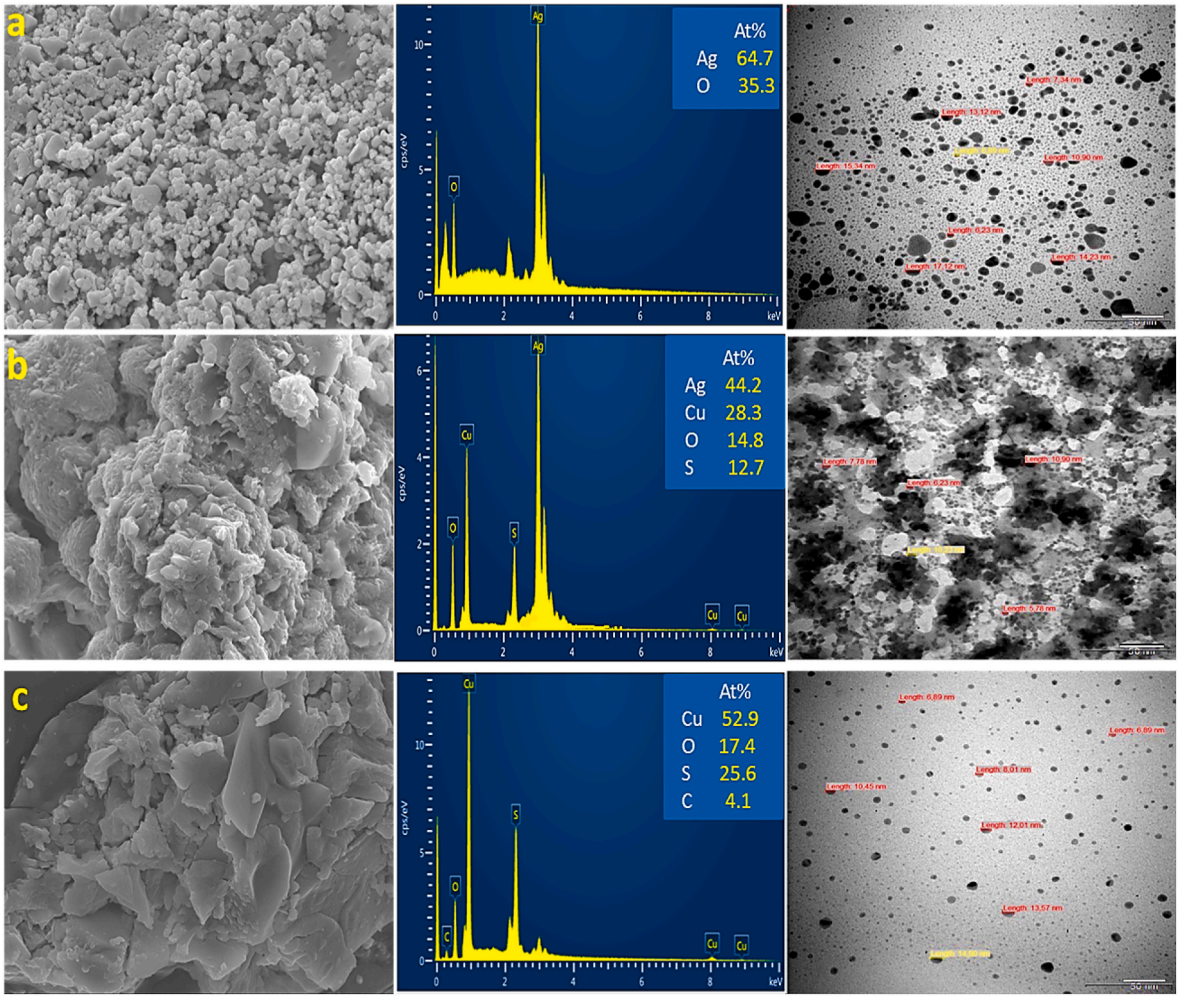

Fig. 3. From left to right SEM, EDX and TEM images of (a) Ag NPs, (b) Ag/Cu NPs and (c) Cu NPs.

Table 2
The specific surface areas and pore parameters of nanoadsorbents/nanocatalysis.

Samples	Specific (BET) surface area (m^2 g^{-1})	Average pore size (nm)	Total pore volume (cm^3 g^{-1})	Relative pressure
Ag NPs	0.155	8.25387	0.000638	0.94983
Ag/Cu NPs	1.123	6.00547	0.003372	0.95174
Cu NPs	12.440	6.87740	0.043130	0.95258

salt. TEM images show that the nanoparticles are spherical.

According to the result of BET analysis given in Table 2, the nanoparticles show the presence of type 4 model and 2–50 nm mesoporous structure in the relative pressure range of 0.5–0.98 [56].

3.2. Adsorption performance of CR onto Ag NPs, Ag/Cu NPs and Cu NPs

Ag NPs, Ag/Cu NPs and Cu NPs nanoadsorbents are used to investigate the adsorption capacity and dye removal percentages for CR. Dye removal percentages after adsorption of 50 mL of 20 mg/L CR dye with 20 mg nanoadsorbents at the end of 120 min are given in Fig. 4a. According to this, it is seen that the best removal percentage is obtained in the presence of Cu NPs with 90.2 %. The UV–Vis spectra of CR adsorption using Cu NPs is given in Fig. 4b. It is observed in Fig. 4c that the adsorption capacity of all adsorbents increased with the increase in dye concentration from 10 to 50 mg/L; however, the increase in Cu NPs is more pronounced and can be attributed to its higher specific surface area compared to both Ag NPs and Ag/Cu NPs. It can be considered that the increase in the initial dye concentration leads to an increase in the mass gradient between the nanoadsorbents and the solution, which is the driving force for its transfer to the surface of the nanoadsorbent [57]. Although the adsorption capacity increased with increasing initial dye concentration, the percent removal decreased (Fig. 4c). Considering the decrease in percent removal efficiency and dye concentration in wastewater, kinetic and isotherm studies are performed with 20 mg/L of CR.

Fig. 4d shows the effect of pH 2–10 on CR adsorption on nanoadsorbents. The results show that the adsorption of CR by all nanoadsorbents is a pH-dependent process. As the pH value increased, the adsorption capacity increased up to pH 6, while the adsorption behaviour decreased after pH 6. Acidic pH was found to increase dye removal due to electrostatic attraction. As pH increases, the number of negatively charged sites increases and the number of positively charged sites decreases. The decrease in adsorption capacity with increasing basicity can be attributed to the ionic repulsion between the anionic dye molecules and the nanoadsorbent surface. In addition, the presence of OH^- ions in the basic solution creates a competitive environment with the anionic ions of CR, resulting in decreased adsorption [58,59]. The effect of adsorbent dosage ranging from 10 to 50 mg on 20 mg/L CR removal increases as shown in Fig. 4d. This increase can be explained by the increase in the adsorption surface area of micropores and the proliferation of adsorption sites [60].

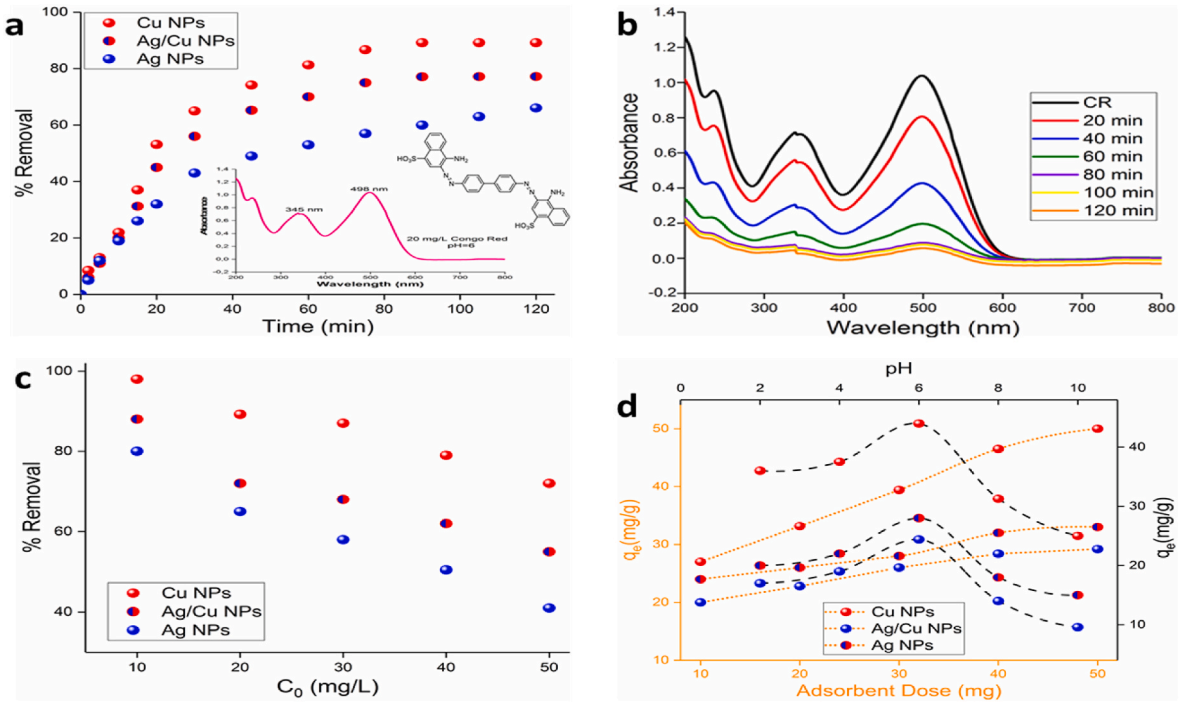

Fig. 4. (a) Comparative CR adsorption of Cu NPs, Ag/Cu NPs and Ag NPs (initial dye concentration: 20 mg/L, adsorbent dosage: 25 mg/50 mL, T = 298 K), (b) UV–Vis spectra of CR adsorption using Cu NPs, (c) Effect of initial dye concentration, on the removal of CR by nanoadsorbents (d) Effect of pH and adsorbent dose on the removal of CR by nanoadsorbents.

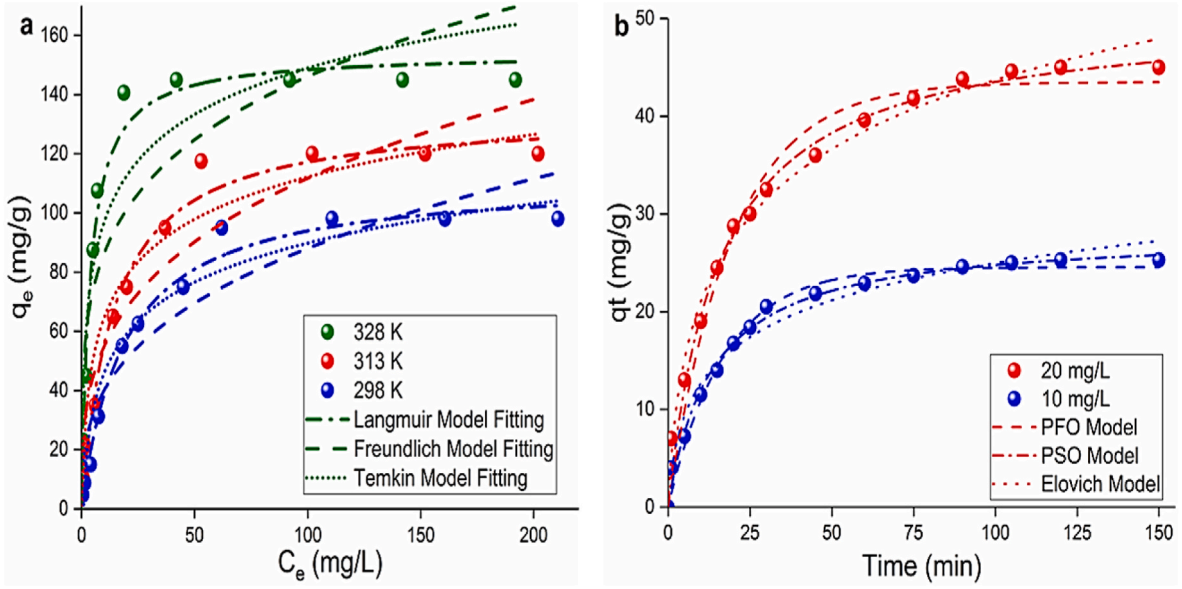

Fig. 5. Adsorption (a) isotherm (b) kinetic of CR onto Cu NPs nanoadsorbents.

Equilibrium studies describe the adsorption isotherm with constants, which are values expressing the affinity and surface properties of adsorbents and determine the capacity of the adsorbent. Langmuir, Freundlich and Temkin adsorption isotherm analyses were performed for Cu NPs, the best adsorbent, to describe the interactions of CR molecules with the surface of the nanoadsorbent (Fig. 5a). Three widely used kinetic models were applied to interpret the experimental data by determining the control mechanism of CR adsorption from aqueous solution (Fig. 5b). The parameters obtained from the kinetic and isotherm plots are given in Table 3.

According to R^2 data in Tables 3 and it is seen that the adsorption fits the second-order kinetic model and Langmuir isotherm model. The fact that the maximum adsorption amount calculated in Table 3 is compatible with the equilibrium adsorption obtained in the experiment supports this result. According to the Langmuir isotherm, adsorption occurs physically and monolayer. The monolayer coating of the CR molecule on the Cu NPs surface can be attributed to the balanced crystal charge of the nanoparticle, little or no displacement between the layers. The larger the K_2 value, the slower the adsorption rate [61]. The pseudo second-order kinetic model assumes that the adsorption rate is determined by the amount of sites remaining on the adsorption surface [62].

As can be seen from the comparative FT-IR and XRD results before

Table 3
Modeling isotherm and kinetic data of CR adsorption on Cu NPs.

Isotherm Model	Parameter & unit	328 K	313 K	298 K	Kinetic Model	Parameter & unit	20 mg/L	10 mg/L
Langmuir	q_m (mg/g)	153.997	133.697	111.710	PFO	q_e (mg/g)	43.5049	24.5649
	K_L (L/mg)	0.26628	0.07111	0.05274		K_1 (1/min)	0.05133	0.05841
	R^2	0.98766	0.98578	0.98906		R^2	0.9787	0.9812
Freundlich	K_F (mg/g)*(mg/L)^n	51.0134	27.0041	18.2940	PSO	q_e (mg/g)	50.3839	28.1182
	1/n	0.22859	0.30839	0.34124		K_2 (g/mg * min)	0.00126	0.00264
	R^2	0.8112	0.9095	0.9036		R^2	0.9986	0.9894
Temkin	B (J/mol)	22.5913	20.6797	19.0830	Elovich	β (mg/g)	0.17832	0.09561
	K_T (L/mg)	7.3022	2.2674	1.1077		α (g/mg * min)	4.77206	6.74234
	R^2	0.9131	0.9506	0.9451		R^2	0.9710	0.9711

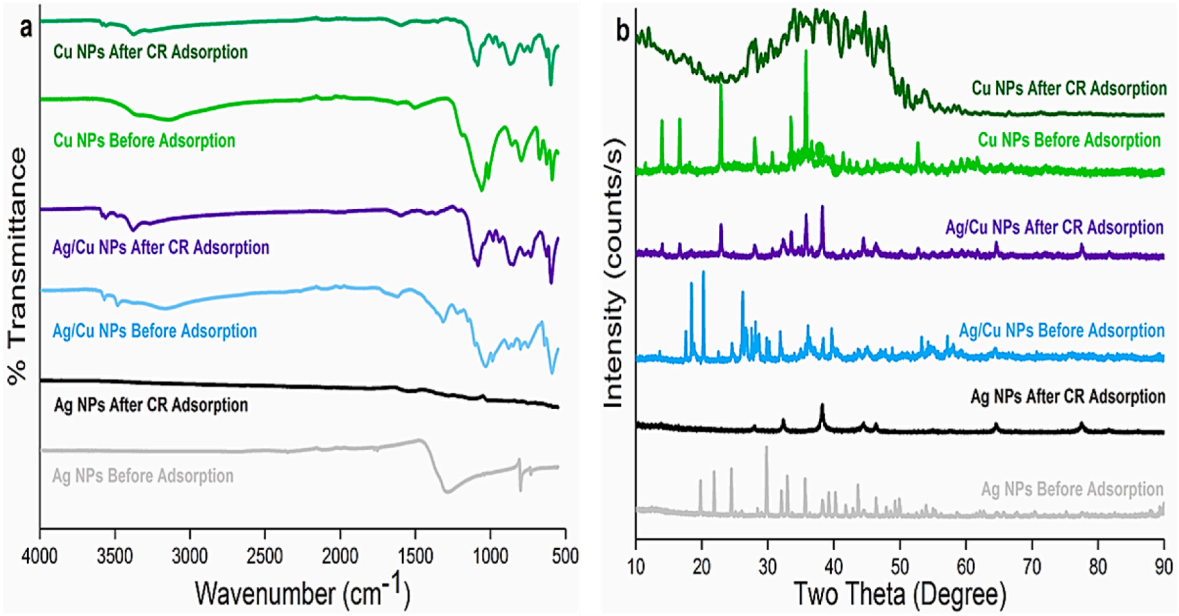

Fig. 6. (a) FTIR spectra (b) XRD models of before and after adsorption CR with Ag NPs, Ag/Cu NPs and Cu NPs.

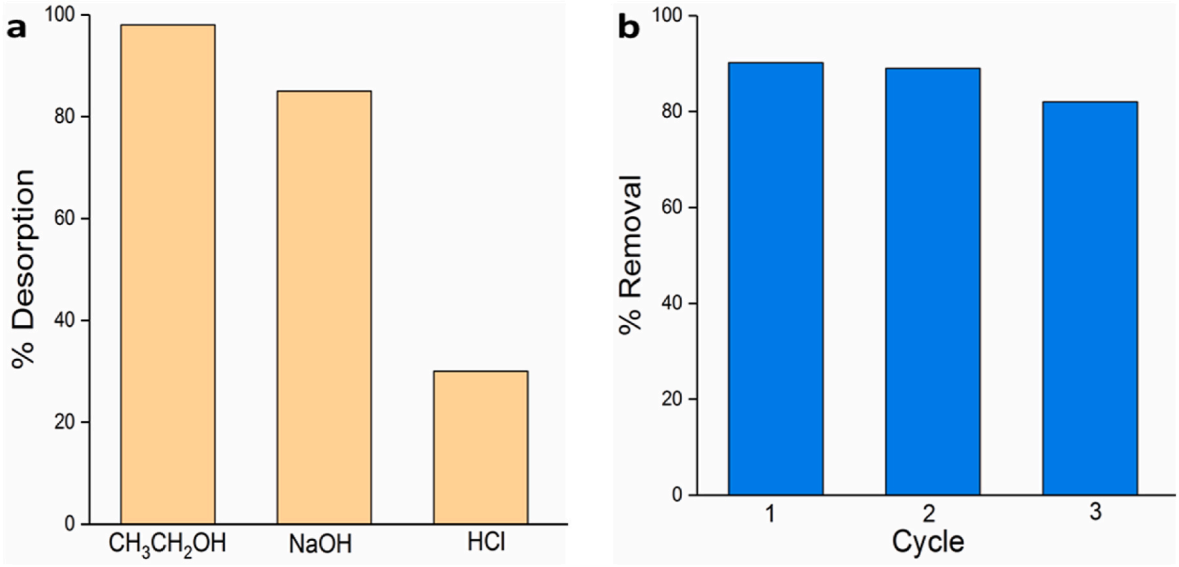

Fig. 7. (a) Desorption (b) Effect of cycles on the adsorption/desorption capacity for CR with Cu NPs.

and after adsorption in Fig. 6, the shift of peak locations and change in peak intensities after adsorption confirm that adsorption has occurred.

CH_3CH_2OH, NaOH and HCl solutions at 0.01 M concentrations were used in the desorption studies to recover CR and test the reusability of the adsorbent and the desorption percentages are given in Fig. 7a. The adsorption/desorption studies were repeated as 3 times to investigate

Table 4
The results of antimicrobial activities of *Helichrysum arenarium* plant extract, Cu NPs, Ag/Cu NPs and Ag NPs.

	Salmonella Typhimurium ATCC 14028	*S. aureus* ATCC 43300	*E. coli* ATCC 25922	*L.monocytogenes* ATCC 19115	*S. aureus* ATCC 25923	*S. epidermidis* ATCC 12228
Extract	0.00 ± 0.00bA	0.00 ± 0.00bA	0.00 ± 0.00 cA	0.00 ± 0.00bA	0.00 ± 0.00 dA	0.00 ± 0.00 cA
Ag NPs	15.50 ± 0.50 aC	17.50 ± 0.50 aB	16.50 ± 0.50aBC	16.00 ± 0.00aBC	20.25 ± 0.25 aA	21.50 ± 0.50 aA
Cu NPs	0.00 ± 0.00bC	0.00 ± 0.00bC	9.00 ± 0.00bB	0.00 ± 0.00bC	10.50 ± 0.50 cA	0.00 ± 0.00 cC
Ag/Cu NPs	14.50 ± 0.50aD	17.00 ± 0.50aABC	16.00 ± 0.00aBCD	15.50 ± 0.50aCD	17.50 ± 0.50bEU	18.50 ± 0.50bA

a-d: The means with different lower letters in each column are statistically significant ($p < 0.05$).
A-D: The means with different upper letters in each row are statistically significant ($p < 0.05$).

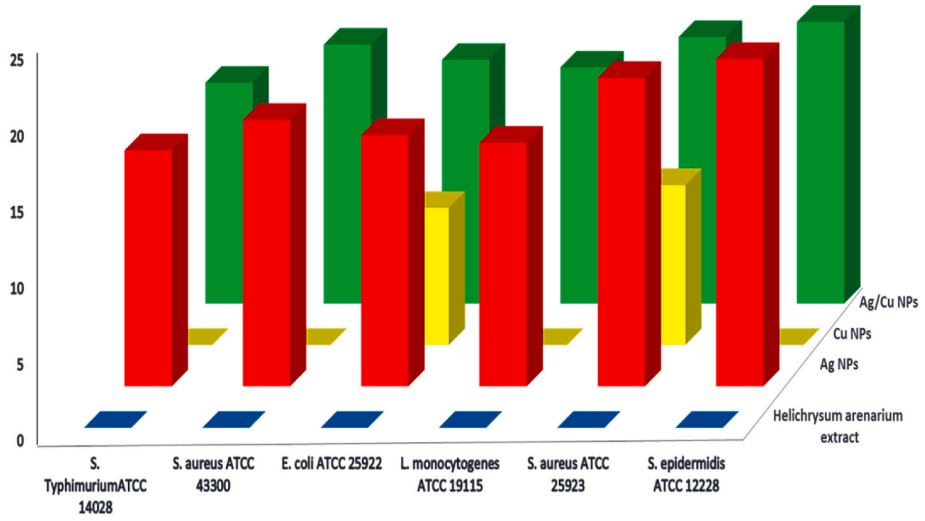

Fig. 8. Antimicrobial activity of *Helichrysum arenarium* plant extract, Cu NPs, Ag/Cu NPs and Ag NPs.

Table 5
Correlation table of inhibition results in pathogen microorganisms.

	S. aureus ATCC 43300	*E. coli* ATCC 25922	*L. monocytogenes* ATCC 19115	*S. aureus* ATCC 25923	S. epidermidis ATCC 12228
Salmonella Typhimurium ATCC 14028	0.999**	0.879**	0.999**	0.875**	0.995**
S. aureus ATCC 43300	–	0.879**	0.999**	0.872**	0.993**
E. coli ATCC 25922		–	0.878**	0.993**	0.875**
L. monocytogenes ATCC 19115			–	0.873**	0.995**
S. aureus ATCC 25923				–	0.878**

*Correlation is significant at the 0.05 level.
**Correlation is significant at the 0.01 level.

the reusability of Cu NPs adsorbent and the results are shown in Fig. 7b. The adsorbent has a stable and active structure and there is a slight decrease in adsorption capacity as can be seen in Fig. 7b.

3.3. Antimicrobial activities

Disk diffusion results of *Helichrysum arenarium* plant extract and nanoparticles in our study are presented in both Table 4 and Fig. 8. According to antimicrobial activity assay, *Helichrysum arenarium* plant extract did not show antimicrobial activity against to the tested pathogen microorganisms. The largest inhibition zone diameter in Ag NPs was found in *S. aureus* (20.25 mm) and *S. epidermidis* (21.50 mm) ($p < 0.05$). In *S. aureus* strains, the antimicrobial effectiveness of Ag NPs decreased in methicillin-resistant strain ($p < 0.05$) is due to the multiple resistance mechanisms shown against methicillin [63]. The largest inhibition diameter of Cu NPs was determined as 10.50 and 9 mm in *S. aureus* and *E. coli*, respectively ($p < 0.05$). No inhibition was found against to other tested pathogenic microorganisms. The smallest inhibition zone of Ag/Cu NPs was detected in *Salmonella* (14.50 mm) ($p < 0.05$). Ag/Cu NPs showed similar inhibition zone diameter in MRSA and *S. aureus*. Ag/Cu NPs also shows that methicillin can be used to control the growth of MRSA.

Table 6
Correlation table of *Helichrysum arenarium* plant extract and nanoparticles.

	Ag NPs	Cu NPs	Ag/Cu NPs
Helichrysum arenarium extract	n	n	n
Ag NPs		0.201	0.901**
Cu NPs			0.148

n: It could not be calculated because at least one of the variables is constant.
*Correlation is significant at the 0.05 level.
**Correlation is significant at the 0.01 level.

The larger inhibition zone diameter of Ag/Cu NPs and Ag NPs were detected in *E. coli*, *L. monocytogenes*, *Salmonella* and MRSA ($p < 0.05$). Pathogenic microorganisms except for *E. coli* (9.00 mm) had no inhibition zone diameter ($p < 0.05$). Both Ag/Cu NPs and Ag NPs showed the largest inhibition diameters in *S. aureus* and *S. epidermidis*, respectively ($p < 0.05$). Cu NPs formed an inhibition zone diameter (10.50 mm) only in *S. aureus* ($p < 0.05$).

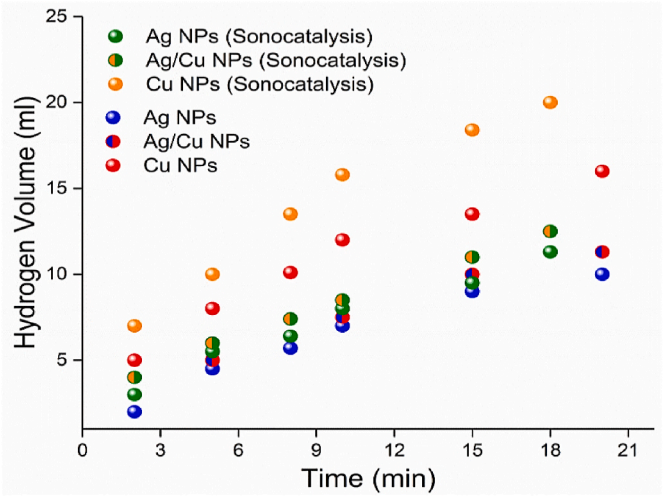

Fig. 9. Hydrolysis of $NaBH_4$ over the Ag NPs, Ag/Cu NPs and Cu NPs catalyst and sonocatalyst

According to the results of the *Pearson correlation test*, the inhibition zone diameters of pathogenic microorganisms show a positive correlation at the 0.01 level (Table 5). The correlation of *Helichrysum arenarium* plant extract, Cu NPs, Ag/Cu NPs and Ag NPs are given in Table 5. Ag/Cu NPs and Ag NPs show a positive correlation at 0.01 level (r:0.901) (see Table 6).

3.4. Hydrogen production by hydrolysis of $NaBH_4$

25 mg of nanocatalyst was placed in a 100 mL of two-necked pyrex glass flask and 50 mL of ultrapure water was added. The glass reactor was placed in a shaking water bath and set at 30 °C and 500 rpm and the shaking water bath was used to keep the ambient temperature under control. A silicone hose was connected to one neck of the reactor and the gas buret was used to allow the hydrogen gas to escape. From the other neck, 25 mL of 50 mg NaOH and 50 mM $NaBH_4$ was added and the mouth of the reactor was closed. The volume of gas released by the hydrogen gas pushing the water in the burette was recorded against time until the gas outlet was terminated. The same process was repeated by treating 25 mg of nanocatalysts with 50 mL of ultrapure water in an ultrasonic bath until homogeneous and the amount of H_2 gas production is given in Fig. 9. It was observed that sonication produced H_2 gas with higher yields in a slightly shorter time. Furthermore, sonication is thought to open the pore diameter or prevent agglomeration.

As seen in Fig. 9, the highest hydrogen production was realized with Cu NPs with the highest surface area and the results are in agreement with the BET analysis. Optimization studies were carried out with Cu NPs and the effects of the changes of the selected parameters on hydrogen gas production are given in Fig. 10.

The optimum parameters for hydrogen production from $NaBH_4$ hydrolysis were determined as 60 °C temperature, 100 mM $NaBH_4$, 50 mg NaOH and 100 mg CuNPs and 30 mL H_2 gas was obtained in 15 min with hydrolysis performed under these optimum conditions. Table 7 shows the comparison of the adsorption capacity in CR removal and the catalytic activity of H_2 production using synthesized nanoparticles with the

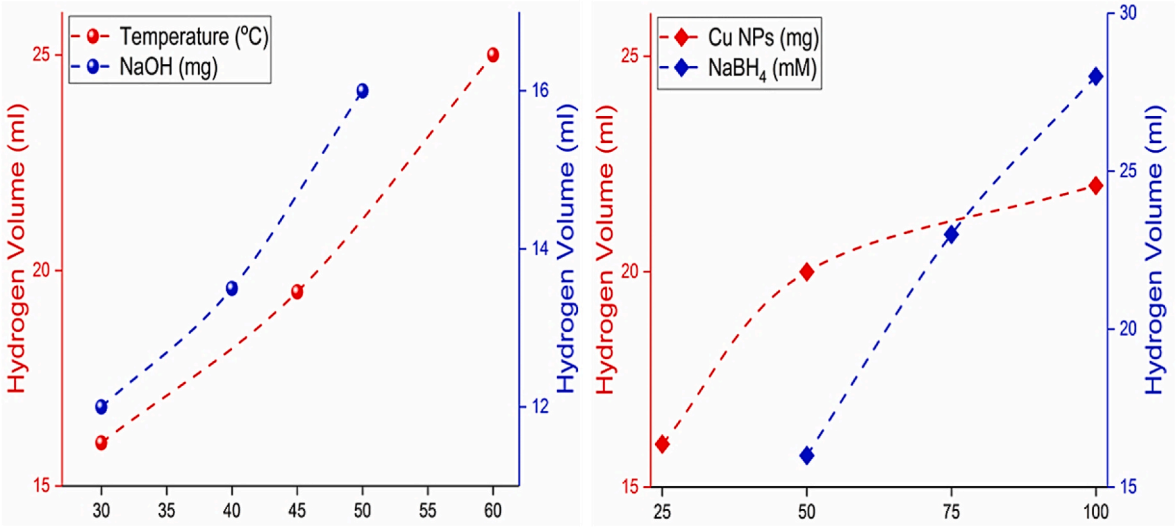

Fig. 10. Generated hydrogen volume versus different temperature and different $NaBH_4$, NaOH and CuNPs concentration.

Table 7
A comparison of CR adsorption capacity of the prepared adsorbent and catalyst in the hydrolysis of $NaBH_4$ for hydrogen production with those announced in the literature.

Adsorbent/Catalyst	H_2 Production Rate (mL)	H_2 Production Time (min)	Adsorption Capacity (mg/g)	Adsorption Contact Time (min)	Reference
Ag@CFC	204	60	–	–	[64]
Cellulose Fibers	250	34	–	–	[65]
Cu@CC	188	6	–	–	[66]
Hydrogel - Co NPs	453	30	–	–	[67]
$NiFe_2O_4$ NPs	–	–	97.1	120	[68]
NFO600	–	–	89.45	1440	[69]
$Co_{0.3}Ni_{0.7}Fe_2O_4$ NPs	–	–	131.75	120	[70]
ZrO_2 hollowspheres	–	–	59.5		[71]
Cu NPs	25	15	153.997	100	Present Study
Ag/Cu NPs	11	15	128.462	100	Present Study
Ag NPs	9	15	102.851	100	Present Study

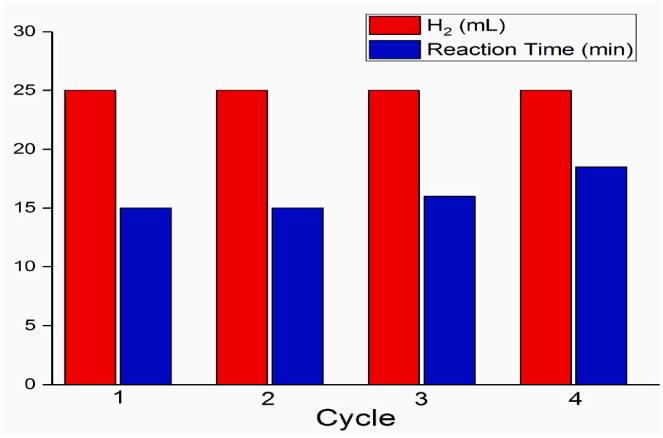

Fig. 11. Effect of cycles on the reaction time and yields for H_2 production with Cu NPs catalyst.

literature values.

Both reusability and hot filtration tests were used to explain the stability and reusability of the catalyst and the heterogeneous nature of the catalysis process. A total of 4 cycles were carried out for the reusability test. After each reaction cycle, Cu NPs nanocatalyst was removed by centrifugation; the separated catalyst was washed thoroughly with alcohol and distilled water and dried at 70 °C for 6 h and used in the next cycle. Fig. 11 shows the H_2 production yield and reaction time after 4 cycles and it can be seen that the yield did not change after the 3rd cycle but the reaction time was increased slightly. The hot filtration test was carried out after the hydrogen production had reached 10 mL and the Cu NPs nanocatalyst was removed under hot conditions by Millex filter with a pore size of 0.2 μm. The remaining liquid was allowed to react for 24 h and it was detected by gas chromatography (GC) that approximately 0.1 mL of H_2 was produced during this time, which is a negligible rate. According to this test, H_2 production stops in the absence of Cu NPs and Cu NPs is an effective catalyst for the hydrogenation reaction.

4. Conclusion

Precious metal containing both metallic and bimetallic nanoparticles were successfully synthesized and characterized by green synthesis method. It was observed that Cu NPs have the highest surface area and pore diameter. Their use as adsorbents for CR dye removal from aqueous solutions was investigated and their antimicrobial properties were also investigated for both cleaner and higher quality water. As a final application, H_2 production and optimization studies were carried out from the synthesized nanoparticles. Sonocatalysis processes were performed to investigate the effect of ultrasonication on agglomeration and pores on nanocatalysts and it was observed that higher H_2 was produced than catalysis processes. Both Ag NPs and Ag/Cu NPs obtained by using *Helichrysum arenarium* plant extract formed an inhibition zone diameter in the tested pathogen microorganisms, while Cu NPs formed an inhibition zone diameter in especially *S.aureus* and *E.coli.* In general, the nanoparticles form a larger inhibition zone diameter in Gram-positive bacteria than in Gram-negative bacteria. Ag/Cu NPs, which forms a similar inhibition zone diameter in *S. aureus* and methicillin-resistant *S. aureus*, will be effective in controlling the growth of resistant microorganisms in water. As a result, it was revealed that Cu NPs have higher dye adsorption capacity (153.997 mg/g) and antimicrobial activity. In addition, 25 mL of H_2 was produced in 15 min after sonication by using Cu NPs as a catalyst in $NaBH_4$ hydrolysis and it is thought that it can be used as a catalyst in H_2 production by developing with natural polymers. The re-usability tests have also shown that Cu NPs can be used as both effective stable adsorbent and catalyst.

CRediT authorship contribution statement

Muradiye Şahin: Data curation, Formal analysis, Resources, Visualization, Writing – original draft, Writing – review & editing. **Yasin Arslan:** Conceptualization, Methodology, Supervision, Writing – review & editing. **Ali Soyuçok:** Writing – original draft.

Declaration of competing interest

The authors declare that they have no known competing financial interests or personal relationships that could have appeared to influence the work reported in this paper.

Data availability

Data will be made available on request.

Acknowledgments

The authors would like to thank to Kırşehir Ahi Evran University Scientific Research Projects (FBE.A4. 22.001) for funding this research.

References

[1] A.M. Ealias, M.P. Saravanakumar, A review on the classification, characterisation, synthesis of nanoparticles and their application, Mater. Sci. Eng. 263 (2017), 032019, https://doi.org/10.1088/1757-899X/263/3/032019.
[2] I. Khan, K. Saeed, I. Khan, Nanoparticles: properties, applications and toxicities, Arab. J. Chem. 12 (2019) 908–931, https://doi.org/10.1016/j.arabjc.2017.05.011.
[3] S. Kumari, L. Sarkar, A Review on nanoparticles: structure, classification, synthesis & applications, J. Sci. Pic. Banaras Hindu University 65 (2021) 42–46, https://doi.org/10.37398/JSR.2021.650809.
[4] M. Vassal, S. Rebelo, MdL Pereira, Metal oxide nanoparticles: evidence of adverse effects on the male reproductive system, Int. J. Mol. Sci. 22 (2021) 8061, https://doi.org/10.3390/ijms22158061.
[5] P.G. Bhavyasree, T.S. Xavier, Green synthesized copper and copper oxide based nanomaterials using plant extracts and their application in antimicrobial activity: review, Curr. Pic. Green and Sustain. Chem. 5 (2022), 100249, https://doi.org/10.1016/j.crgsc.2021.100249.
[6] N.G. Girón-Vázquez, C.M. Gómez-Gutiérrez, C.A. Soto-Robles, O. Nava, E. Lugo-Medina, V.H. Castrejón-Sánchez, A.R. Vilchis-Nestor, P.A. Luque, Study of the effect of Persea americana seeds in the green synthesis of silver nanoparticles and their antimicrobial properties, Results Phys 13 (2019), 102142, https://doi.org/10.1016/j.rinp.2019.02.078.
[7] Y. Liu, R. Pei, Z. Huang, J. Xiao, A. Yao, K. Xu, Y. Li, S. Ullah, Z. Yu, Y. Wang, S. F. Zhou, G. Zhan, Green immobilization of CdS-Pt nanoparticles on recombinant Escherichia coli boosted by overexpressing cysteine desulfurase for photocatalysis application, Bioresour. Technol. Rep. 16 (2021), 100823, https://doi.org/10.1016/j.biteb.2021.100823.
[8] M. Şahin, İ.H. Gübbük, Synthesis of antioxidant silver nanoparticles, characterization and catalysis applications, Int. J. Adv. Eng. Pure Sci. 31 (2019) 75–83, https://doi.org/10.7240/jeps.497405.
[9] S. Vijayakumar, S. Mahadevan, P. Arulmozhi, S. Sriram, P.K. Praseetha, Green synthesis of zinc oxide nanoparticles using Atalantia monophylla leaf extracts: characterization and antimicrobial analysis, Mater. Sci. Semicond. Process. 82 (2018) 39–45, https://doi.org/10.1016/j.mssp.2018.03.017.
[10] M. Şahin, Y. Arslan, F. Tomul, Removal of naproxen and diclofenac using magnetic nanoparticles/nanocomposites, Res. Chem. Intermed. 48 (2022) 5209–5226, https://doi.org/10.1007/s11164-022-04862-y.
[11] M. Kaur, D.S. Chopra, Green synthesis of iron nanoparticles for biomedical applications, Globe. J. Nanomed. 4 (2018) 68–77, https://doi.org/10.19080/GJN.2018.04.555643.
[12] Z. Markova, P. Novak, J. Kaslik, P. Plachtova, M. Brazdova, D. Jancula, K. M. Siskova, L. Machala, B. Marsalek, R. Zboril, Iron (II, III)-polyphenol complex nanoparticles derived from green tea with remarkable ecotoxicological impact, ACS Sustain. Chem. Eng. 2 (2014) 1674–1680, https://doi.org/10.1021/sc5001435.
[13] M. Nasrollahzadeh, N.S.S. Bidgoli, Z. Issaabadi, Z. Ghavamifar, T. Baran, R. Luque, Hibiscus Rosasinensis L. aqueous extract-assisted valorization of lignin: preparation of magnetically reusable Pd NPs@Fe_3O_4-lignin for Cr(VI) reduction and Suzuki-Miyaura reaction in eco-friendly media, Int. J. Biol. Macromol. 148 (2020) 265–275, https://doi.org/10.1016/j.ijbiomac.2020.01.107.
[14] M. Şahin, M. Atasoy, Y. Arslan, D. Yıldız, Removal of Ni (II), Cu (II), Pb (II), and Cd (II) from aqueous phases by silver nanoparticles and magnetic nanoparticles/nanocomposites, ACS Omega 8 (2023) 34834–34843, https://doi.org/10.1021/acsomega.3c04054.
[15] T. Cherian, K. Ali, B. Saquib, M. Faisal, R. Wahab, J. Musarrat, Cymbopogon citratus functionalized green synthesis of CuO-nanoparticles: novel prospects as

antibacterial and antibiofilm agents, Biomolecules 10 (2020) 169–175, https://doi.org/10.3390/biom10020169.
[16] N.T.T. Nguyen, L.M. Nguyen, T.T.T. Nguyen, U.P.N. Tran, D.T.C. Nguyen, T. V. Tran, A critical review on the bio-mediated green synthesis and multiple applications of magnesium oxide nanoparticles, Chemosphere 312 (2023), 137301, https://doi.org/10.1016/j.chemosphere.2022.137301.
[17] M. Nasrollahzadeh, F. Ghorbannezhad, Z. Issaabadi, S.M. Sajadi, Recent developments in the biosynthesis of Cu-based recyclable nanocatalysts using plant extracts and their application in the chemical reactions, Chem. Rec. 19 (2019) 601–643, https://doi.org/10.1002/tcr.201800069.
[18] B.N. Rashmi, S.F. Harlapur, B. Avinash, C.R. Ravikumar, H.P. Nagaswarupa, M. R. Anil Kumar, K. Gurushantha, M.S. Santosh, Facile green synthesis of silver oxide nanoparticles and their electrochemical, photocatalytic and biological studies, Inorg. Chem. Commun. 111 (2020), 107580, https://doi.org/10.1016/j.inoche.2019.107580.
[19] B. Adebayo-Tayo, A. Salaam, A. Ajibade, Green synthesis of silver nanoparticle using Oscillatoria sp. extract, its antibacterial, antibiofilm potential and cytotoxicity activity, Helion 5 (2019), 02502, https://doi.org/10.1016/j.heliyon.2019.e02502.
[20] T. Bruna, F. Maldonado-Bravo, P. Jara, N. Caro, Silver nanoparticles and their antibacterial applications, Int. J. Mol. Sci. 22 (2021) 7202, https://doi.org/10.3390/ijms22137202.
[21] N. Nagar, V. Devra, Activation of peroxodisulfate and peroxomonosulfate by green synthesized copper nanoparticles for Methyl Orange degradation: a kinetic study, J. Environ. Chem. Eng. 5 (2017) 5793–5800, https://doi.org/10.1016/j.jece.2017.11.014.
[22] S. Rajeshkumar, G. Rinitha, Nanostructural characterization of antimicrobial and antioxidant copper nanoparticles synthesized using novel Persea americana seeds, OpenNano 3 (2018) 18–27, https://doi.org/10.1016/j.onano.2018.03.001.
[23] A. Mosbah, H. Chouchane, S. Abdelwahed, A. Redissi, M. Hamdi, S. Kouidhi, M. Neifar, A. Slaheddine Masmoudi, A. Cherif, W. Mnif, Peptides fixing industrial textile dyes: a new biochemical method in wastewater treatment, J. Chem. 2019 (2019), 5081807, https://doi.org/10.1155/2019/5081807.
[24] S. Pai, M.S. Kini, R. Selvaraj, A review on adsorptive removal of dyes from wastewater by hydroxyapatite nanocomposites, Environ. Sci. Pollut. Pic. 28 (2021) 11835–11849, https://doi.org/10.1007/s11356-019-07319-9.
[25] A. Tkaczyk, K. Mitrowska, A. Posyniak, Synthetic organic dyes as contaminants of the aquatic environment and their implications for ecosystems: a review, Sci. Total Environ. 717 (2020), 137222, https://doi.org/10.1016/j.scitotenv.2020.137222.
[26] M.J. Uddin, R.E. Ampiaw, W. Lee, Adsorptive removal of dyes from wastewater using a metal-organic framework: a review, Chemosphere 284 (2021), 131314, https://doi.org/10.1016/j.chemosphere.2021.131314.
[27] N. Tara, S.I. Siddiqui, G. Rathi, S.A. Chaudhry, A.M. Asiri, Nano-engineered adsorbent for the removal of dyes from water: a review, Curr. Anal. Chem. 16 (2020) 14–40, https://doi.org/10.2174/1573411015666190117124344.
[28] H. Balouchi, M. Baziar, A. Dehghan, H. Alidadi, M. Shams, Combination of electrocoagulation and MOF adsorption systems for EBT removal from water, Int. J. Environ. Anal. Chem. 102 (2020) 1307–1317, https://doi.org/10.1080/03067319.2020.1737035.
[29] Q. Zhao, C. Zhang, X. Tong, Y. Zou, Y. Li, F. Wei, Fe_3O_4-NPs/orange peel composite as magnetic heterogeneous Fenton-like catalyst towards high-efficiency degradation of methyl orange, Water Sci. Technol. 84 (2021) 159–171, https://doi.org/10.2166/wst.2021.221.
[30] L.D. Ardila-Leal, R.A. Poutou-Piñales, A.M. Pedroza-Rodríguez, B.E. Quevedo-Hidalgo, A brief history of colour, the environmental impact of synthetic dyes and removal by using laccases, Molecules 26 (2021) 1–40, https://doi.org/10.3390/molecules26133813.
[31] V. Katheresan, J. Kansedo, S.Y. Lau, Efficiency of various recent wastewater dye removal methods: a review, J. Environ. Chem. Eng. 6 (2018) 4676–4697, https://doi.org/10.1016/j.jece.2018.06.060.
[32] C. Amor, L. Marchão, M.S. Lucas, J.A. Peres, Application of advanced oxidation processes for the treatment of recalcitrant agro-industrial wastewater: a review, Water 11 (2019) 1–31, https://doi.org/10.3390/w11020205.
[33] S.A.R. Khan, P. Ponce, Z. Yu, H. Golpîra, M. Mathew, Environmental technology and wastewater treatment: strategies to achieve environmental sustainability, Chemosphere 286 (2022), 131532, https://doi.org/10.1016/j.chemosphere.2021.131532.
[34] M. Kurian, Advanced oxidation processes and nanomaterials-a review, Clean. Eng. Technol. 2 (2021), 100090, https://doi.org/10.1016/j.clet.2021.100090.
[35] A. Hassani, M. Malhotra, A.V. Karim, S. Krishnan, P.V. Nidheesh, Recent progress on ultrasound-assisted electrochemical processes: a review on mechanism, reactor strategies, and applications for wastewater treatment, Environ. Pic. 205 (2022), 112463, https://doi.org/10.1016/j.envres.2021.112463.
[36] K.Q. Jabbar, A.A. Barzinjy, S.M. Hamad, Iron oxide nanoparticles: preparation methods, functions, adsorption and coagulation/flocculation in wastewater treatment, Environ. Nanotechnol. Monit. Manag. 17 (2022), 100661, https://doi.org/10.1016/j.enmm.2022.100661.
[37] M. Shkir, B. Palanivel, A. Khan, M. Kumar, J.H. Chang, A. Mani, S. AlFaify, Enhanced photocatalytic activities of facile auto-combustion synthesized ZnO nanoparticles for wastewater treatment: an impact of Ni doping, Chemosphere 291 (2022), 132687, https://doi.org/10.1016/j.chemosphere.2021.132687.
[38] P.S. Goh, K.C. Wong, A.F. Ismail, Membrane technology: a versatile tool for saline wastewater treatment and resource recovery, Desalination 521 (2022), 115377, https://doi.org/10.1016/j.desal.2021.115377.
[39] Y. Vieira, M.S. Netto, É.C. Lima, I. Anastopoulos, M.L. Oliveira, G.L. Dotto, An overview of geologically originated materials as a trend for adsorption in wastewater treatment, Geosci. Front. 13 (2022), 101150, https://doi.org/10.1016/j.gsf.2021.101150.
[40] B. Chen, F. Long, S. Chen, Y. Cao, X. Pan, Magnetic chitosan biopolymer as a versatile adsorbent for simultaneous and synergistic removal of different sorts of dyestuffs from simulated wastewater, Chem. Eng. J. 385 (2020), 123926, https://doi.org/10.1016/j.cej.2019.123926.
[41] Y. Zhou, J. Lu, Y. Zhou, Y. Liu, Recent advances for dyes removal using novel adsorbents: a review, Environ. Pollut. 252 (2019) 352–365, https://doi.org/10.1016/j.envpol.2019.05.072.
[42] E.M. Nigri, A.L.A. Santos, S.D.F. Rocha, Removal of organic compounds, calcium and strontium from petroleum industry effluent by simultaneous electrocoagulation and adsorption, J. Water Process Eng. 37 (2020), 101442, https://doi.org/10.1016/j.jwpe.2020.101442.
[43] R. Kishor, D. Purchase, G.D. Saratale, R.G. Saratale, L.F.R. Ferreira, M. Bilal, R. Chandra, R.N. Bharagava, Ecotoxicological and health concerns of persistent coloring pollutants of textile industry wastewater and treatment approaches for environmental safety, J. Environ. Chem. Eng. 9 (2021), 105012, https://doi.org/10.1016/j.jece.2020.105012.
[44] S. Lamichaney, R.K. Baranwal, S. Maitra, G. Majumdar, Clean energy technologies: hydrogen power and fuel cells, reference module in mater, Sci. Mater. Eng. 3 (2020) 366–371, https://doi.org/10.1016/B978-0-12-803581-8.11040-9.
[45] B. Jaleh, M. Nasrollahzadeh, A. Nasri, M. Eslamipanah, A. Moradi, Z. Nezafat, Biopolymer-derived (nano)catalysts for hydrogen evolution via hydrolysis of hydrides and electrochemical and photocatalytic techniques: a review, Int. J. Biol. Macromol. 182 (2021) 1056–1090, https://doi.org/10.1016/j.ijbiomac.2021.04.087.
[46] M. Eslamipanah, B. Jaleh, B.F. Mohazzab, S. Khazalpour, M. Nasrollahzadeh, M. Shokouhimehr, Facile synthesis and electrochemical hydrogen storage of bentonite/TiO_2/Au nanocomposite, Int. J. Hydrogen Energy 45 (2020) 33771–33788, https://doi.org/10.1016/j.ijhydene.2020.09.044.
[47] M. Nasrollahzadeh, M. Maham, M.M. Tohidi, Green synthesis of water-dispersable palladium nanoparticles and their catalytic application in the ligand- and copper-free Sonogashiracoupling reaction under aerobic conditions, J. Mol. Catal. Chem. 391 (2014) 83–87, https://doi.org/10.1016/j.molcata.2014.04.004.
[48] M. Xiong, Z. Gao, Y. Qin, Spillover in heterogeneous catalysis: new insights and opportunities, ACS Catal. 11 (2021) 3159–3172, https://doi.org/10.1021/acscatal.0c05567.
[49] A. Nasri, B. Jaleh, S. Khazalpour, M. Nasrollahzadeh, M. Shokouhimehr, Facile synthesis of graphitic carbon nitride/chitosan/Au nanocomposite: a catalyst for electrochemical hydrogen evolution, Int. J. Biol. Macromol. 164 (2020) 3012–3024, https://doi.org/10.1016/j.ijbiomac.2020.08.143.
[50] A. Sápi, T. Rajkumar, J. Kiss, Á. Kukovecz, Z. Kónya, G.A. Somorjai, Metallic nanoparticles in heterogeneous catalysis, Catal. Lett. 151 (2021) 2153–2175, https://doi.org/10.1007/s10562-020-03477-5.
[51] M. Şahin, Y. Arslan, Adsorptive and oxidative removal of naproxen and diclofenac using Ag NPs, Cu NPs and Ag/Cu NPs, Res. Chem. Intermed. 49 (2023) 3627–3643, https://doi.org/10.1007/s11164-023-05048-w.
[52] R. Komal, V. Arya, Biosynthesis and characterization of silver Nanoparticles from aqueous leaf extracts of carica Papaya and its antibacterial activity, Int. J. Nanomater. Biostruct. 3 (2013) 17–20.
[53] M. Nasrollahzadeh, S.M. Sajadi, A. Hatamifard, Waste chicken eggshell as a natural valuable resource and environmentally benign support for biosynthesis of catalytically active Cu/eggshell, Fe_3O_4/eggshell and Cu/Fe_3O_4/eggshell nanocomposites, Appl. Catal., B 191 (2016) 209–227, https://doi.org/10.1016/j.apcatb.2016.02.042.
[54] M. Nasrollahzadeh, Z. Issaabadi, S.M. Sajadi, Green synthesis of Cu/Al_2O_3 nanoparticles as efficient and recyclable catalyst for reduction of 2,4-dinitrophenylhydrazine, Methylene blue and Congo red, Composites, Part B 166 (2019) 112–119, https://doi.org/10.1016/j.compositesb.2018.11.113.
[55] S. Chaudhary, D. Rohilla, A. Umar, N. Kaur, A. Shanavas, Synthesis and characterizations of luminescent copper oxide nanoparticles: toxicological profiling and sensing applications, Ceram. Int. 45 (2019) 15025–15035, https://doi.org/10.1016/j.ceramint.2019.04.239.
[56] S. Guo, G. Zhang, J. Wang, Photo-Fenton degradation of rhodamine B using Fe_2O_3 - kaolin as heterogeneous catalyst: characterization, process optimization and mechanism, J. Colloid Interface Sci. 433 (2014) 1–8, https://doi.org/10.1016/j.jcis.2014.07.017.
[57] V. Vimonses, S. Lei, B. Jin, C.W.K. Chow, C. Saint, Kinetic study and equilibrium isotherm analysis of Congo Red adsorption by clay materials, Chem. Eng. J. 148 (2009) 354–364, https://doi.org/10.1016/j.cej.2008.09.009.
[58] L. Ai, Y. Zeng, Hierarchical porous NiO architectures as highly recyclable adsorbents for effective removal of organic dye from aqueous solution, Chem. Eng. J. 215 (2013) 269–278, https://doi.org/10.1016/j.cej.2012.10.059.
[59] C. Lei, X. Zhu, B. Zhu, J. Yu, W. Ho, Hierarchical NiO-SiO_2 composite hollow microspheres with enhanced adsorption affinity towards Congo red in water, J. Colloid Interface Sci. 466 (2016) 238–246, https://doi.org/10.1016/j.jcis.2015.12.035.
[60] I.D. Mall, V.C. Srivastava, N.K. Agarwal, I.M. Mishra, Removal of Congo red from aqueous solution by bagasse fly ash and activated carbon: kinetic study and equilibrium isotherm analyses, Chemosphere 61 (2005) 492–501, https://doi.org/10.1016/j.chemosphere.2005.03.065.
[61] J. Wang, X. Guo, Adsorption isotherm models: classification, physical meaning, application and solving method, Chemosphere 258 (2020), 127279, https://doi.org/10.1016/j.chemosphere.2020.127279.
[62] H. Li, V.L. Budarin, J.H. Clark, M. North, X. Wu, Rapid and efficient adsorption of methylene blue dye from aqueous solution by hierarchically porous, activated

starbons®: mechanism and porosity dependence, J. Hazard Mater. 436 (2022), 129174, https://doi.org/10.1016/j.jhazmat.2022.129174.
[63] A. Soyuçok, The effects of some essential oils on methicillin resistant Staphylococcus aureus, Turkish J. Agric-Food Sci. Technol. 10 (2022) 49–53, https://doi.org/10.24925/turjaf.v10i1.49-53.4831.
[64] F. Ali, S.B. Khan, A.M. Asiri, Enhanced H_2 generation from $NaBH_4$ hydrolysis and methanolysis by cellulose micro-fibrous cottons as metal templated catalyst, Int. J. Hydrogen Energy 43 (2018) 6539–6550, https://doi.org/10.1016/j.ijhydene.2018.02.008.
[65] F. Ali, S.B. Khan, A.M. Asiri, Chitosan coated cellulose cotton fibers as catalyst for the H2 production from NaBH4 methanolysis, Int. J. Hydrogen Energy 44 (2019) 4143–4155, https://doi.org/10.1016/j.ijhydene.2018.12.158.
[66] S.B. Khan, Metal nanoparticles containing chitosan wrapped cellulose nanocomposites for catalytic hydrogen production and reduction of environmental pollutants, Carbohydr. Polym. 242 (2020), 116286, https://doi.org/10.1016/j.carbpol.2020.116286.
[67] S. Chairam, P. Jarujamrus, M. Amatatongchai, Starch hydrogel-loaded cobalt nanoparticles for hydrogen production from hydrolysis of sodium borohydride, Adv. Nat. Sci. Nanosci. Nanotechnol. 10 (2019), 025013, https://doi.org/10.1088/2043-6254/ab23fb.
[68] L. Wang, J. Li, Y. Wang, L. Zhao, Q. Jiang, Adsorption capability for Congo red on nanocrystalline MFe_2O_4 (M = Mn, Fe, Co, Ni) spinel ferrites, Chem. Eng. J. 181 (2012) 72–79, https://doi.org/10.1016/j.cej.2011.10.088.
[69] C. Kong, J. Li, F.T. Liu, Y. Song, P. Song, Synthesis of $NiFe_2O_4$ using degreasing cotton as template and its adsorption capacity for Congo Red, Desalination Water Treat. 57 (2016) 11337–11347, https://doi.org/10.1080/19443994.2015.1043589.
[70] R. Chen, W. Wang, X. Zhao, Y. Zhang, S. Wu, F. Li, Rapid hydrothermal synthesis of magnetic $Co_XNi_{1-X}Fe_2O_4$ nanoparticles and their application on removal of Congo red, Chem. Eng. J. 242 (2014) 226–233, https://doi.org/10.1016/j.cej.2013.12.016.
[71] C. Wang, Y. Le, B. Cheng, Fabrication of porous ZrO_2 hollow sphere and its adsorption performance to Congo red in water, Ceram. Int. 40 (2014) 10847–10856, https://doi.org/10.1016/j.ceramint.2014.03.078.